THE ASTRONOMICAL JOURNAL VOLUME 87, NUMBER 12 DECEMBER 1982

VISUAL AND INFRARED OBSERVATIONS OF THE DISTANT COMETS P/STEPHAN-OTERMA (1980g), PANTHER (1980u), AND BOWELL (1980b)[a]

D. C. JEWITT
Palomar Observatory and the Division of Geological and Planetary Sciences, California Institute of Technology, Pasadena, California 91125

B. T. SOIFER, G. NEUGEBAUER, AND K. MATTHEWS
Palomar Observatory and the Division of Physics, Mathematics and Astronomy, California Institute of Technology, Pasadena, California 91125

G. E. DANIELSON[b]
Palomar Observatory and the Division of Geological and Planetary Sciences, California Institute of Technology, Pasadena, California 91125

Received 28 May 1982; revised 17 August 1982

ABSTRACT

Broadband observations of comets P/Stephan-Oterma (1980g), Bowell (1980b), and Panther (1980u) in the visual [$0.5 \lesssim \lambda$ (μm) $\lesssim 0.9$] and infrared [$1.2 \lesssim \lambda$ (μm) $\lesssim 20$] wavelength regions are reported together with measurements in the 1.5–2.4-μm wavelength range having 5% spectral resolution. The visual data indicate the existence of solid grains in extended halos around the nuclei of the three comets. The visual photometric profiles of comets P/Stephan-Oterma and Panther are interpreted as evidence that grains around Panther and those close to the nucleus of P/Stephan-Oterma are sublimating. Broadband near-infrared and thermal infrared measurements of comet Panther suggest the presence of 2–4-μm radius particles in the coma. The particles within a 5.8×10^6-m diameter region centered on the comet have a total cross section of 10^8 m^2 and a near-infrared geometric albedo of about 14%. Comet Bowell presents a total cross section of 3×10^8 m^2 within a 1.2×10^7-m region centered on the comet and its coma grains also have an albedo of 14%. The near-infrared spectrum of P/Stephan-Oterma is a featureless solar-reflection continuum. The near-infrared spectra of Bowell and Panther exhibit features which are similar in the two comets. The spectral features are not due to H_2O, CH_4, or CO_2 ices nor to emissions from gases released from the nuclei nor to reflection from mineral grains of known composition in the comae. The spectrum of solid ammonia provides the best match to the near infrared; it is nevertheless significantly different from the comet spectra. The synthesis of the visual data with the infrared data is attempted in terms of a model involving a mantle of volatile material on the nuclei of Bowell and Panther, but not on P/Stephan-Oterma. The composition of the mantle cannot be exactly specified from the existing data but a complex molecule incorporating the N–H bond may be present.

I. INTRODUCTION

Comet nuclei are generally supposed to consist of heterogeneous mixtures primarily of water ice and refractory dust grains (Whipple 1950, 1951). The thermodynamic properties of water ice are such that the gross features of cometary activity are well matched by a water-based model. Quantities of more complex materials must be present in order to account for spectroscopic identifications of C, C_2, C_3, HCN, CO, and numerous other radicals in comet comae and tails. Recent observations of H_2O^+ (Wehinger *et al.* 1974), and of appropriate quantities of H and O, support the notion that H_2O dominates the composition of comet nuclei. However, an unambiguous direct detection of H_2O molecules in any comet has yet to be reported.

At intermediate heliocentric distances [$2 \lesssim R$ (AU) $\lesssim 10$] many comets exhibit activity in excess of that expected from a sublimating water nucleus. Modification of the canonical model by replacing water snow by clathrates of volatile molecules does not remove this problem: the sublimation rate of a CO_2 clathrate, for instance, is similar to that of water ice itself since the water ice lattice must be disrupted before the CO_2 can escape (Delsemme and Miller 1970). Most likely frozen volatiles are responsible for the excess activity but their identity is unknown. The problem is especially acute for many of the long-period "first appearance" comets which are frequently active at $R > 2$ AU. Two of the comets discussed in this work (Bowell and Panther) fall into this class. The other (P/Stephan-Oterma) is a short-period object.

Although the above dilemma between theory and observation has been recognized for many years, few attempts have been made to resolve it by observational

[a] Contribution No. 3694 from the Division of Geological and Planetary Sciences, California Institute of Technology, Pasadena, California 91125.

[b] Guest Observer, Kitt Peak National Observatory, Tucson, Arizona 85726.

 0004-6256/82/121854-13$00.90

means. Broadband infrared observations have been taken from numerous comets (Becklin and Westphal 1966; O'Dell 1971; Ney 1975). Only two attempts have been made to detect the near-infrared spectral features of ices in comets. Oishi *et al.* (1978) failed to detect any such features in comet West because the 3-μm region of the comet spectrum was contaminated by strong thermal emission. More recently A'Hearn *et al.* (1981) examined P/Stephan-Oterma and obtained a reflection spectrum devoid of features but similar to the spectrum reported in the present work. Because of the large diaphragm used by these observers, it is likely that the near-infrared spectrum they obtained refers to refractory grains in the outer coma and not to ice grains in a cloud near the nucleus. In this paper we report combined visual imagery and spectroscopy, near-infrared spectroscopy, and broadband infrared photometry of the three mentioned comets at intermediate heliocentric distances.

II. OBSERVATIONS AT VISUAL WAVELENGTHS

Observations in the visual range [$0.5 \lesssim \lambda$ (μm) $\lesssim 0.9$] were obtained with the CCD camera built by the Space Telescope Wide Field and Planetary Camera Investigation Definition Team (Gunn and Westphal 1981). The camera ("PFUEI") enables rapid interchange between operation as a direct camera and as a low-resolution ($\lambda / \Delta\lambda \sim 250$) visual spectrograph. PFUEI was used at the prime focus of the Hale 5.1-m telescope and at the Cassegrainian focus of the 1.5-m telescope, both at Palomar Observatory, and at the Cassegrainian focus of the 2.1-m telescope at KPNO. A journal of observations, together with a list of relevant camera parameters is given in Table I.

The characteristics of the PFUEI which are especially relevant to the comet imaging include the seeing-limited spatial resolution (commonly 1–2 arcsec), the good linearity of the detector response (0.1%), the great sensitivity (the quantum efficiency of the detector averages 0.5 at $\lambda \sim 0.6$ μm), and the large dynamic range. The latter is especially important for studies near the photometric nuclei of the comets where the coma surface brightness may vary greatly over short distances. In the spectrographic mode a 105×2-arcsec slit was used.

In addition to the data frames listed in Table I, numerous flat field and erase frames were recorded. These were subsequently used to remove the zero-exposure bias signal from the CCD chip and to divide out pixel-to-pixel variations in the sensitivity. The processed data frames are generally found to be uniform at the 1% level over their full width. Defective pixels remain imperfectly "flattened" but are, however, so few in number ($< 0.1\%$ of the total) as to be largely negligible. When precision photometry was performed, the defective pixels were eliminated by replacing them with the average value of the four adjacent pixels. Processed data frames are limited by photon noise. Occasionally several consecutive frames were digitally stacked to improve the signal-to-noise ratio. The stars BD + 26°2606, BD + 29°2091, BD + 54°1216, HD 84937, and HD 19445 were recorded to provide measures of the absolute surface brightnesses of the comets (Thuan and Gunn 1978).

The appearances of the comets through broadband filters with bandpasses ~ 0.1 μm and central wavelengths 0.50, 0.65, 0.80, and 0.95 μm were similar. Unless otherwise noted the following descriptions apply to all filters but refer specifically to data taken with the 0.65-μm filter. Table II lists the heliocentric distance R, geocentric distance Δ, and phase angle α for each comet at the first and last dates of observation.

The photometric profiles of the comets were examined by taking brightness averages within concentric circular annuli about the photometric centers of the comae. Representative results are plotted in Fig. 1. The ordinate is the logarithm of the surface brightness B above the sky background B_s (in arbitrary units). On the abscissa is plotted the logarithm of the radial distance from the photometric center in arcseconds. The error bars represent the maximum uncertainties associated with the determination of the sky background. Statistical uncertainties in the coma signal are negligible as are errors due to imperfect location of the photometric center. Where errors are not plotted, it is because they are too small to be shown at the scale of the graph.

a) P/Stephan-Oterma

The main feature of this comet was an almost stellar brightness enhancement around the location of the nu-

TABLE I. Journal of visual observations.

Date	Telescope diameter (m)	Image scale (arcsec per pixel)	Seeing (arcsec)	Direct frames[a]	Spectra[a]
12/17/80	1.5	0.59	1–2	S-O	S-O
12/18/80	1.5	0.59	2	S-O, B	S-O
2/18/81 to 2/23/81	1.5	0.59	1–2.5	S-O, B	B
3/21/81	5.1	0.42	5	—	P, S-O
5/6/81	2.1	0.46	1.5	P	—
5/18/81	1.5	0.59	1–2	S-O, B	—

[a] S-O = Stephan-Oterma, B = Bowell, P = Panther.

TABLE II. Supporting comet information.

Comet	Period of observations	R (AU)	Δ (AU)	α (degs)
P/Stephan-Oterma	12/15/80–5/19/81	1.58–2.59	0.60–2.52	3–23
Bowell	12/18/80–5/19/81	5.34–4.38	5.42–3.73	10–11
Panther	3/21/81–5/6/81	1.80–2.10	1.42–2.11	33–27

cleus. This is shown in Fig. 2 by a brightness profile across the nuclear region of the comet and across a typical field star. The extended wings at the base of the comet profile are due to the extended coma. The full width of half-maximum (FWHM) of the nuclear region (1.58 ± 0.03 arcsec) was found to be significantly larger than the FWHM of nearby field stars (1.40 ± 0.03 arcsec), indicating the presence of a 0.7 ± 0.1-arcsec [$(8 \pm 1) \times 10^5$-m diameter] cloud around the nucleus. The enhanced nuclear region was observed in frames obtained December 1980 through May 1981, though the degree of enhancement decreased during this period. In mid-February 1981 the material in the resolved nuclear region had an albedo cross-section product equal to 8.0×10^7 m^2, as judged by aperture photometry from CCD frames. Out to a radius of 10 arcsec ($\sim 10^7$ m), the isophotes of the coma remain closely circular.

Visual spectra of the coma and nuclear region of comet P/Stephan-Oterma show a bright solar reflection continuum with a few weak emissions from [O I] and C_2 (Fig. 3). Between 0.5 and 0.7 μm the gaseous emissions contribute $< 1\%$ to the total brightness of the comet in February 1981 data.

b) Comet Panther

Comet Panther displayed a bright coma, spherically symmetric out to $\sim 10^7$ m. No nuclear condensation was seen (see Fig. 1). The albedo cross-section product within a circular aperture of 2×10^7-m projected radius was 1.7×10^8 m^2; this value may be uncertain by up to 50% since the comet was observed on a night of low photometric quality.

Visual slit spectra of comet Panther reveal many prominent spectral lines and bands. These are shown in Fig. 3, together with several line identifications. An estimated 1% of the total light between 0.5 and 0.7 μm was gaseous emission, the remainder was reflection continuum.

c) Comet Bowell

This comet displayed a large bright coma in all filters. Its photometric profile, shown in Fig. 1, gives no evidence for a strong central condensation. The material within 2×10^7 m of the nucleus had an albedo cross-section product equal to 1.0×10^8 m^2, similar to that

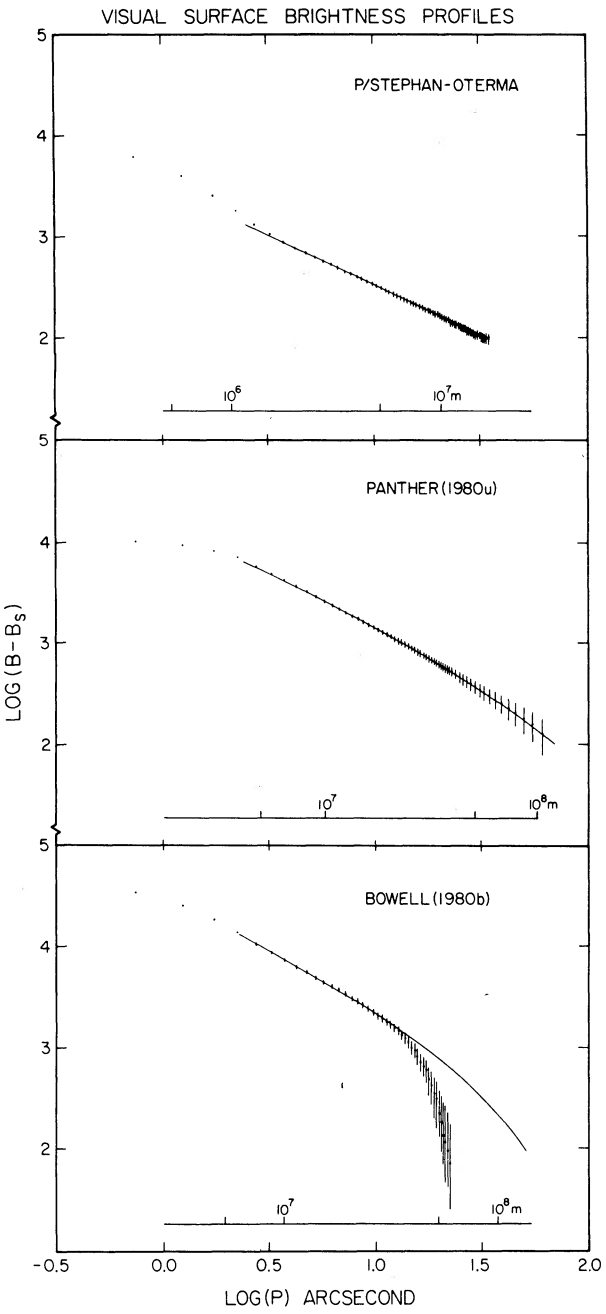

FIG. 1. Logarithmic brightness profiles of the three comets at 0.65-μm wavelength. The ordinate is proportional to the logarithm of the surface brightness of the coma above the sky background. The coma surface brightness was averaged around concentric annuli centered on the nucleus. The logarithm of P, the radius of the annulus in arcseconds, is plotted on the abscissa. For clarity, only about half of the measured data points have been plotted for each comet. The continuous lines represent model fits described in the text. The fits to the surface brightness B are not plotted for $\log p < 0.4$ or for $B - B_s < 0.1 B_s$, where B_s is the sky background brightness. In each graph, $B_s \sim 10^3$ data numbers. The three profiles were measured from CCD images taken 12/17/80, 5/6/81, and 2/20/81, respectively.

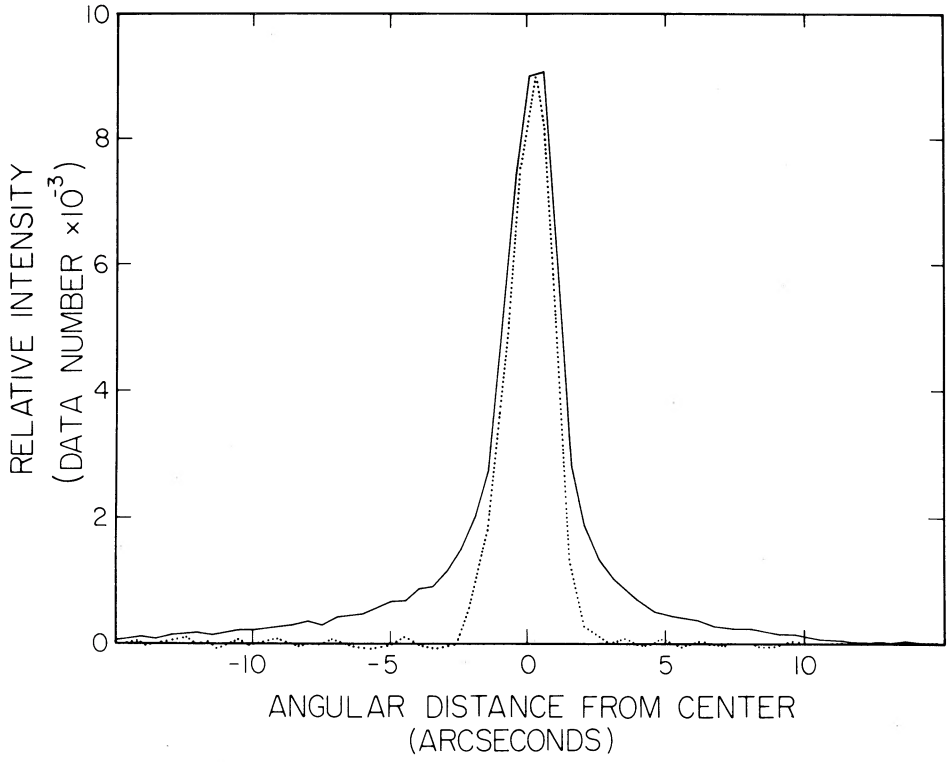

FIG. 2. Brightness profiles across the central region of comet P/Stephan-Oterma (solid line) and across a star image (dotted line) are taken from a single CCD frame. The pixel size is 0.59 arcsec. In addition to having broad "wings" due to coma, the comet profile has a FWHM significantly larger than the 1.40 ± 0.03-arcsec FWHM of the star image. A central "cloud" $(8 \pm 1) \times 10^5$-m diameter is present in the comet. The profile was measured from a CCD image taken on 12/17/80 with the Palomar 1.5-m telescope.

present in the nuclear excess of P/Stephan-Oterma alone. A faint stubby tail extending in the antisolar direction was evident in the PFUEI data. The contribution of the tail to the total light of the comet was estimated to be $< 5\%$.

Visual spectra taken with the slit across the nuclear region of the comet reveal a solar reflection continuum completely devoid of gaseous emissions, typical of many comets at such large heliocentric distance ($R = 5$ AU in February 1981).

III. SPECTRAL OBSERVATIONS AT NEAR-INFRARED WAVELENGTHS

Comets P/Stephan-Oterma and Panther were observed in the near infrared on UT 16 March 1981 using the Palomar 5-m telescope. Observations of comet Bowell were acquired on UT 14 April 1981. The infrared observations were obtained with an InSb detector cooled to 55 K and a circular variable filter (CVF) wheel cooled to 77 K. The spectra had a resolution $\lambda / \Delta\lambda \sim 20$. Photometric observations were obtained successively at wavelengths separated by half-resolution intervals. For the Bowell and Panther observations a 6-arcsec diameter diaphragm was used with 6-arcsec chop in the north-south direction to remove infrared background radiation. In the case of P/Stephen-Oterma a smaller diaphragm of 3 arcsec was used with a 3-arcsec chop in the north-south direction. The smaller diaphragm was selected in order to maximize the contribution to the signal from the central excess of P/Stephan-Oterma (cf. Sec. II a). This accounts for the relatively large errors in the spectrum of the latter object as compared with those in the Panther and Bowell spectra. Except for the measurements of comet Bowell between 1.46 and 1.78 μm, the measurements, summarized in Table III, are averages of two or three values obtained in consecutive wavelength scans. In each case the individual scans were similar within the statistical uncertainties. The conversion to absolute flux density was achieved through observations of early-type stars at similar airmasses. The spectra were divided by the solar spectrum as measured by Arveson *et al.* (1969) to obtain relative reflectivities. The relative reflectivities of the three comets normalized to unity at 2.20 μm are presented in Fig. 4.

The near-infrared relative reflectivities of Bowell and Panther are identical within the uncertainties. Both comets exhibit a broad reflectivity minimum centered at 2.22 ± 0.02 μm. Reflectivity maxima at 1.78, 2.15, and > 2.40 μm are common to both objects, as is a trend of increasing reflectivity with wavelength.

Although the similarity between the reflectivities of comets Bowell and Panther is clear, it is less clear whether the P/Stephan-Oterma reflectivities agree with or significantly differ from those of Panther or Bowell, especially in view of the larger uncertainties on the former. The value of $\chi^2 = 17$ was computed between the mean Panther-Bowell and P/Stephan-Oterma spectra. The number of data points was 17. The chance that this value of χ^2 (or a larger one) would result from measure-

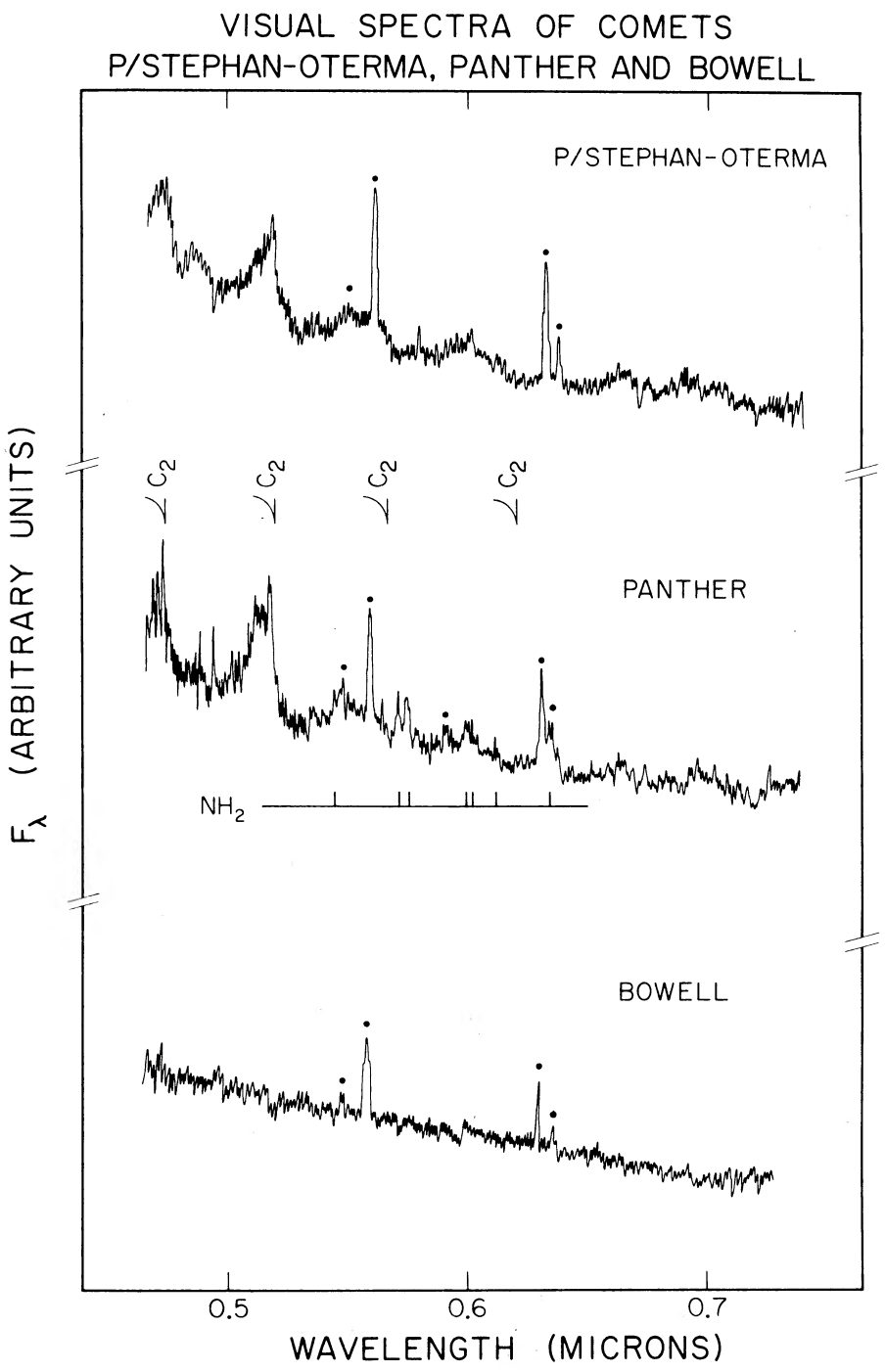

FIG. 3. Visual spectra obtained from CCD frames. The ordinates are proportional to the flux density at each wavelength. C_2 bandheads and NH_2 emission lines are identified. Lines partly or wholly due to night sky emission are marked with dots. The spectrum of P/Stephan-Oterma was taken on 12/18/80 with the Palomar 1.5-m telescope, while the spectra of comets Panther and Bowell were taken with the Palomar 5-m telescope on 3/21/81 and 2/21/81, respectively.

TABLE III. Measured near-infrared flux densities.

Wavelength (μm)	Stephan-Oterma (mJy)	Bowell (mJy)	Panther (mJy)
1.46	—	3.87 ± 0.29	—
1.50	1.22 ± 0.08	4.12 ± 0.14	28.4 ± 0.4
1.54	1.19 ± 0.08	3.95 ± 0.10	27.3 ± 0.4
1.58	1.30 ± 0.08	3.97 ± 0.13	26.8 ± 0.4
1.62	1.18 ± 0.07	4.09 ± 0.08	26.4 ± 0.4
1.66	1.15 ± 0.03	3.71 ± 0.09	26.3 ± 0.4
1.70	1.21 ± 0.05	3.95 ± 0.08	26.2 ± 0.4
1.74	1.11 ± 0.05	3.61 ± 0.07	26.6 ± 0.4
1.78	1.22 ± 0.04	3.66 ± 0.16	28.0 ± 0.4
2.00	0.90 ± 0.04	2.78 ± 0.06	20.0 ± 0.3
2.05	0.88 ± 0.03	2.85 ± 0.06	19.9 ± 0.3
2.10	0.92 ± 0.03	2.81 ± 0.06	19.5 ± 0.3
2.15	0.79 ± 0.03	2.75 ± 0.09	19.7 ± 0.3
2.20	0.88 ± 0.05	2.65 ± 0.07	19.0 ± 0.3
2.25	0.99 ± 0.04	2.54 ± 0.06	18.1 ± 0.3
2.30	0.82 ± 0.06	2.39 ± 0.09	17.6 ± 0.3
2.35	0.76 ± 0.06	2.48 ± 0.11	18.7 ± 0.3
2.40	0.77 ± 0.04	2.50 ± 0.12	17.9 ± 0.3
2.45	—	2.50 ± 0.26	—

ments of identical spectra is ~ 0.4. Hence the P/Stephan-Oterma spectrum has the same shape as the average Panther-Bowell spectrum within the uncertainties. A'Hearn *et al.* (1981) have also measured the near-infrared spectrum of P/Stephan-Oterma but used a 10-arcsec diaphragm. Using their reflectivities to compare P/Stephan-Oterma with Panther gives $\chi^2 = 18$ from 17 data points: again there is ~ 0.4 chance that the P/Stephan-Oterma and Panther-Bowell reflectivities are the same. Hence the P/Stephan-Oterma spectrum is consistent with the Panther and Bowell spectra within the uncertainties of the measurements.

IV. BROADBAND INFRARED WAVELENGTH OBSERVATIONS

Comets Panther and Bowell were observed through broadband infrared filters on the nights of UT 14 and 15 April 1981. Again the Palomar 5-m telescope was used. The filters employed had central wavelengths 1.2, 1.6, 2.2, 3.7, 4.8, 10, and 20 μm. The first five of these filters had fractional FWHM bandpasses of $\sim 20\%$. The 10- and 20-μm filters had bandpasses of about 6 μm. A diaphragm of 4.4 arcsec diameter was employed. The measurements were reduced to absolute flux densities by using observations of stars on the photometric system defined by Elias *et al.* (1982). The broadband data are summarized in Table IV and are plotted in Fig. 5. In the figure a broadband observation at 0.65 ± 0.1 μm, obtained by summing over an effective 4.4-arcsec diameter diaphragm, has been added for comparison with the infrared data. This flux density, derived by comparison with the photometric standards of Sec. II, was found to be 0.9 ± 0.1 mJy.

V. INTERPRETATION OF THE VISUAL DATA

In this section an attempt is made to use the appearances of the comets as seen in the PFUEI direct images and visual spectra to help define the properties of the three objects.

It may be noted that the visual data do not refer to the bare nuclei of the comets. Having typical radii of a few kilometers (Wyckoff 1982), such nuclei would be observed as unresolved objects having geometric albedo cross-section products of less than about 10^7 m^2. No such objects are seen in any of the comets. Instead the light is scattered from their comae.

We take the strong continua in the visual spectra shown in Fig. 3 to indicate that most of the light from the three comets is sunlight scattered from solid particles. The emission bands and lines observed in comet Panther can be attributed to the C_2 and NH_2 radicals.

Comparisons of the observed logarithmic visual brightness profiles of the three comets with model calculations are physically revealing. In making such comparisons the parts of the profiles with $\log p \lesssim 0.4$ and with $B - B_s < 0.1 B_s$ are ignored; here p is the angular separation, in arcseconds, between the photometric center of the coma and the line of sight, and $B - B_s$ is the brightness of the coma above the sky brightness B_s. In the former region the observed profiles are distorted by the effects of atmospheric seeing while in the latter region errors in the choice of the sky brightness become significant.

In the simplest model the coma comprises an isotropically expanding spherically symmetric and optically thin collection of constant-size dust grains. In such a coma the grain number density n varies with radial distance from the center of the nucleus, r, according to $n \propto r^{-2}$ as a consequence of continuity. The coma surface brightness then varies as $B(p) \propto p^{-1}$. This result remains valid for an optically thin coma even for nonisotropic grain ejection, provided the ejection is symmetric about the subsolar point on the nucleus and provided observations are made from small phase angles. Numerical integrations show that the first-order effects of the distortion of the coma by solar radiation pressure do not alter the above result.

This very simple coma model is plotted in the upper part of Fig. 1, where it is seen to provide a satisfactory fit to the observed brightness profile of P/Stephan-Oterma. The success of this simple model is taken to indicate that the coma of P/Stephan-Oterma, for $\log p > 0.4$, consists of a steadily expanding collection of grains each of constant radius. However, at $\log p \lesssim 0.3$ the surface brightness rises considerably higher than the projected $B(p) \propto p^{-1}$ variation. This excess cannot be a result of the seeing: the smearing action of the seeing would instead tend to depress the observed brightness. The central brightness excess must result from an excess grain cross section in the region around the nucleus. The most likely explanation of the brightness excess which is consistent with its observed persistence (at least five months) and with its finite width is that it is an ice grain halo (Delsemme and Miller 1971). Individual ice grains ejected from the nucleus by gas drag sublimate in the

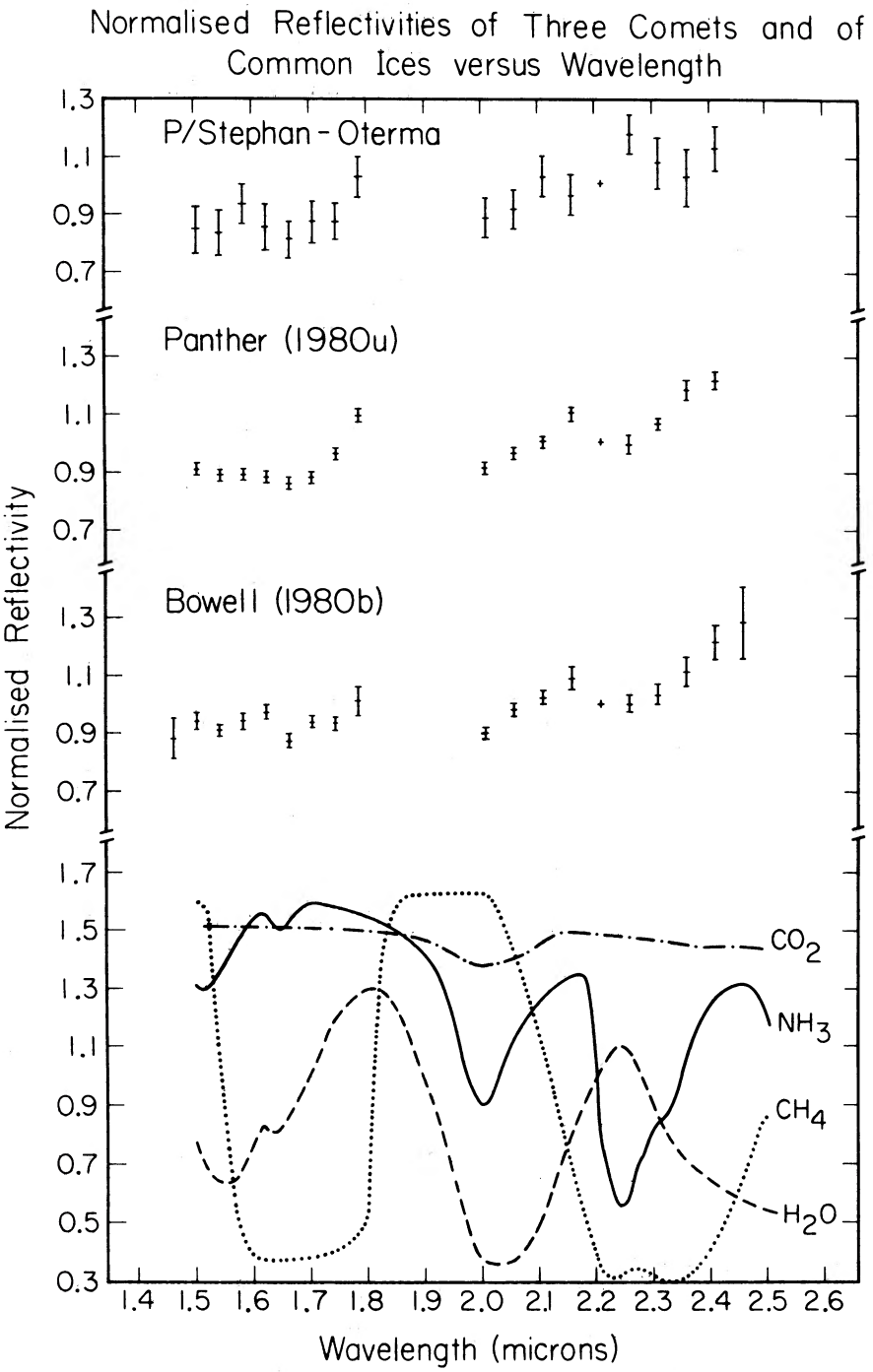

FIG. 4. Near-infrared reflectivities obtained by dividing the cometary flux densities by the solar flux density. The comet reflectivities have been normalized at 2.2 μm. The laboratory spectra of ice are arbitrarily normalized. A 3-arcsec diaphragm and 3-arcsec beam chop were used for the observations of comet P/Stephan-Oterma in order to suppress the contribution from the isotropic coma and to enhance that from the nuclear excess. The spectra of comets P/Stephan-Oterma and Panther were obtained on 3/16/81. The spectrum of comet Bowell was obtained on 4/14/81. All observations were with the Palomar 5-m telescope.

TABLE IV. Broadband infrared measurements.

λ (μm)	Panther Flux density (mJy)	Bowell Flux density (mJy)
1.2	12 ± 1	3.5 ± 0.3
1.6	12 ± 1	3.2 ± 0.2
2.2	8.4 ± 0.6	2.1 ± 0.2
3.7	8 ± 2	—
4.8	60 ± 20	—
10	870 ± 100	17 ± 2
20	2500 ± 600	400 ± 200

sunlight and all but disappear by the time they have traveled a few hundred kilometers. Refractory grains which may be incorporated within the ice grains are "released" at the edge of the ice grain halo and travel outward to populate the isotropic region observed at $\log p > 0.4$. The persistence of the ice grain halo is due to its continual replenishment by sublimation of the nucleus. Dirty water ice grains of initial radius $a(0) \sim 100$ μm would indeed have lifetimes of a few hours, permitting them to travel the observed 400-km radius of the halo (Hanner 1980).

Attempts to fit the profiles of comets Bowell and Panther with the simple isotropic expansion model are unsatisfactory. We therefore attempt to reproduce the observed profiles with a model involving sublimating grains following the approach of Delsemme and Miller (1971). The grain radius at distance r from the nucleus is

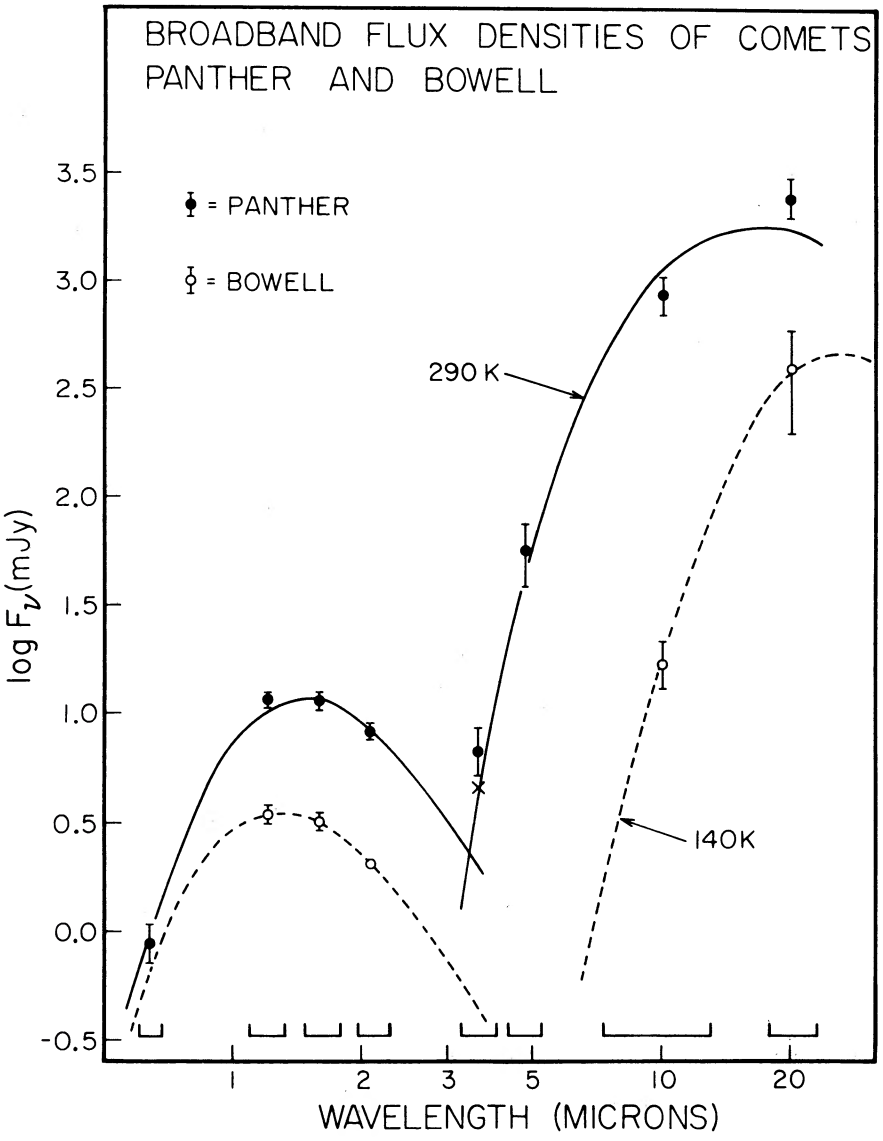

FIG. 5. The logarithms of the broadband flux densities (in mJy) are plotted vs the central wavelengths (in μm). All observations were made with a 4.4-arcsec diaphragm. The filter FWHM are indicated by horizontal bars. Continuous and dashed lines are blackbody fits to the reflected and thermal components of the two spectra. The broadband measurements were obtained on 4/14/81 and 4/15/81 with the 5-m telescope.

put equal to

$$a(r) = a(0)[1 - r/r_H], \quad (1)$$

where $a(0)$ is the initial radius of the grain and r_H is the radius of the ice grain halo. Equation (1) merely implies that the grain size decreases at a constant rate, approximately consistent with grain sublimation for instance, or with sputtering erosion. More complicated alternatives to Eq. (1) could be substituted but would be difficult to justify.

By integrating along the line of sight, it may be shown that Eq. (1) leads to a coma surface brightness

$$B(\gamma) = A\left[\frac{\arccos\gamma}{\gamma} - 2\ln\left(\frac{1+(-\gamma^2)^{1/2}}{\gamma}\right) + (1-\gamma^2)^{1/2}\right], \quad (2)$$

where $\gamma = p/p_H, 0 < \gamma \leqslant 1, p_H$ is the angular radius of the ice grain halo in arcseconds, and A is a constant.

Equation (2) has been fitted to the observed profiles by varying p_H and the constant of proportionality. The best-fit lines are plotted in the middle and lower parts of Fig. 1. A fit to P/Stephan-Oterma is indistinguishable from the fit obtained using the simple model, provided the ice grain halo radius is $p_H \gtrsim 10^4$ arcsec ($r_H \gtrsim 5\times 10^9$ m). In the case of comet Panther, the fit achieved with Eq. (2) is entirely satisfactory (see Fig. 1). The ice grain halo radius deduced from the fit is $p_H = 320$ arcsec ($r_H = 5\times 10^8$ m). The good fit strongly suggests that the coma around Panther consists of an expanding halo of grains composed of a sublimating volatile material.

The fit to the profile of comet Bowell is less pleasing (see Fig. 1). The surface brightness of this comet decreases much more rapidly with p than would that of an ice grain halo. We do not understand the surface brightness profile of comet Bowell. Sekanina (1981) has suggested that the coma of Bowell in fact comprises a swarm of large particles *in orbit* about the nucleus, in which case the ice grain halo model would be inapplicable. The present data neither confirm nor deny this contention and it would seem prudent to reserve judgment on the nature of the coma particles until better observations and/or models are available.

It has already been noted that solar radiation pressure would not substantially affect the near-nucleus brightness profiles of the cometary comae. However, another argument concerning the effects of radiation pressure may be used to constrain estimates of the grain sizes. To first order the effect of a radiation-pressure-induced acceleration w would be to move an initially circular dust shell radially back a distance $l \sim \frac{1}{2}w(r/v)^2$, where r is the radius of the dust shell in question and v is the initial speed of ejection of the dust grains into the coma. The distances l and r may be measured from the PFUEI images. The velocity v may be estimated from Bobrovnikoff's (1954) empirical relation

$$v\ (\mathrm{m\ s^{-1}}) \sim 500R^{-0.6}, \quad (3)$$

where R is the heliocentric distance measured in AU. Since Eq. (3) describes the motions of shocks in the gaseous components of comae, we may confidently use it to provide *upper limits* to the speeds of solid grains and so upper limits to the radiation-pressure-induced accelerations. Values of l, R, and v are listed in Table V, together with the resultant accelerations w. The ratio $\beta = w/g_\odot$, with $g_\odot$ the local acceleration due to solar gravity, is also listed for each comet.

The ratio β depends upon the grain radius a, on the mass density ρ, and on the grain complex refractive index $m = n - ik$. Values of β vs a have been computed for a number of common solar system materials by Burns *et al.* (1979). From their Fig. 1 it may be observed that the upper limits to β found for comets Panther and Stephan-Oterma rule out the substantial presence of iron or magnetite grains between about 0.02- and 0.4-μm radius. More specific statements concerning the particle sizes cannot be made from the visual data alone.

VI. INTERPRETATION OF THE BROADBAND INFRARED DATA

In Fig. 5 the reflected and thermally radiated components of the radiation from comets Panther and Bowell are clearly separated. At $\lambda \lesssim 3\ \mu$m the measured flux densities are due to sunlight scattered by the coma grains. At $\lambda \gtrsim 4\ \mu$m the measured radiation is primarily due to sunlight absorbed and then reradiated by the grains. The measurement of comet Panther at 3.7 μm represents mostly thermal radiation but contains a significant component due to reflected solar radiation. By fitting a Planck function to the points with $\lambda < 3\ \mu$m and extrapolating to 3.7 μm, the reflected solar radiation component was estimated to be 3 mJy, leaving 5 mJy of thermal emission. The effective blackbody temperature of the reflected radiation, $\sim$3000 K, is forced by the low flux density at 0.65 μm, and implies an intrinsic redness of the grains. The 3.7-μm measurement corrected for the reflected component is indicated in Fig. 5 by a cross.

Planck functions were fitted to the thermal broadband measurements of the two comets. The resulting best fits are shown in the figure. There is no evidence for the 10-μm emission normally associated with the presence of silicates in comets. However, at the relatively large heliocentric distances of comets Panther and Bowell, the emission is not expected. In the case of com-

TABLE V. Measurements of coma distortion.

Parameter[a]	Stephan-Oterma	Bowell	Panther
l[b]	1.5×10^6	3.7×10^7	1.6×10^6
r (m)	1.7×10^7	4.7×10^7	1.8×10^7
R (AU)	1.83	4.90	2.10
v (m s^{-1})[c]	350	190	320
w (m s^{-2})	$<1.3\times10^{-3}$	$<1.2\times10^{-3}$	$<1.0\times10^{-3}$
$g_\odot$ (m s^{-2})	1.8×10^{-3}	2.5×10^{-4}	1.35×10^{-3}
β	<0.7	<5	<0.8

[a] See Sec. V.
[b] Projection factor included.
[c] Computed with Eq. (3).

et Bowell the best-fit temperature is estimated to be 140 ± 10 K, where the uncertainty results mostly from the uncertainty on the 20-μm data point. This may be compared to the temperature expected for a blackbody at the same 4.6-AU heliocentric distance, namely $T_{BB} = 130$ K. The two temperatures are in agreement. However, the best-fit temperature for comet Panther is 290 ± 15 K, which is $\sim 50\%$ higher than the equilibrium blackbody temperature $T_{BB} = 210$ K at $R = 1.8$ AU.

This detection of elevated grain temperature can be used to limit the range of grain properties in the coma of comet Panther by the following method. The elevated grain temperature implies that the emissivities of the grains must decrease with increasing wavelength. The specific form of the wavelength dependence can be found from the solution of the thermal equilibrium condition for individual grains. If the grains can be treated as spheroidal Mie particles, the thermal equilibrium condition is

$$\int_0^\infty Q_a(a,\lambda,m)F_\odot(\lambda)\,d\lambda = 4\pi R^2 \int_0^\infty Q_a(a,\lambda,m)B(\lambda,T)\,d\lambda, \quad (4)$$

where $Q_a(a,\lambda,m)$ is the absorption efficiency of a grain of radius a and complex refractive index m at wavelength λ, $F_\odot(\lambda)$ is the solar flux density at a heliocentric distance of 1 AU, R is the heliocentric distance of the grain in AU, and $B(\lambda,T)$ is the Planck function at temperature T. Equation (4) was solved iteratively for the $Q_a(a,\lambda,m)$. To facilitate the evaluation of Eq. (4), the solar flux density $F_\odot(\lambda)$ was approximated by a 5890-K blackbody. Because the refractive index m of the grain material is unknown, the equation was solved for a range of complex indices of astrophysical interest. After each iteration the Mie particle emission spectrum was fitted to the long-wavelength broadband measurements in order to compute the new best-fit temperature. The iterations were halted when the change in grain temperature between successive iterations became less than the temperature uncertainty due to the errors on the broadband measurements themselves. Usually three iterations were found to be sufficient. The corresponding size uncertainties typically amount to a few tenths of a micron. For complex refractive indices $m = n - ik$, with n in the range 1.1–1.5 and k in the range 0.07–0.3, the equilibrium grain radii were found to lie in the range from 2 to 4 μm. The physical temperatures corresponding to these particles were close to 250 K.

Particles with radii around 2–4 μm have small β values which are consistent with the upper limit imposed by the visual data. At visual and near-infrared wavelengths the particles have $x = 2\pi a/\lambda \gg 1$ and would thus be considered large in the classical sense. In the 10-μm thermal emission region the particles have $x \sim 1$.

It would not be reasonable to attempt to reach more specific conclusions than those above since (a) the cometary grains are probably not well approximated by Mie spheriods, (b) the size distribution of the grains is unknown, (c) the complex refractive indices of the grains are unknown, and (d) the quality of the broadband data does not permit a study significantly more detailed than the present one.

The observed thermal flux densities can be used to compute the cross section present in the coma from the absorption efficiency $Q_a(a,\lambda,m)$. Under the safe assumption of an optically thin coma, the total cross section present within a 4.4-arcsec diameter diaphragm (corresponding to 5.8×10^6 m at the comet) is $(1.0 \pm 0.2) \times 10^8$ m^2. The observed near-infrared broadband measurements then give the near-infrared albedo as 0.14 ± 0.05.

It may be noted that the broadband observations permit an estimate of the total mass of the dust in the coma of comet Panther. The total cross section was found to be $\sim 1 \times 10^8$ m^2. With a grain radius of 4 μm some 2×10^{18} grains were present in the coma. If the grain density was 10^3 kg m^{-3}, the total mass of the grains within a region subtending 5.6×10^6 m centered on the nucleus was 5×10^5 kg. From Eq. (3) an upper limit to the expansion speed of the grains from the nucleus of 350 m s^{-1} may be obtained. This implies the time within the diaphragm to be $> 8 \times 10^3$ s and an upper limit to the mean grain mass production rate to be approximately 60 kg s^{-1}. Averaged over the surface of a 10^3-m radius nucleus, this is equivalent to an upper limit to the surface recession rate of 5×10^{-9} m s^{-1}. This rate could be sustained for years before substantial depletion of the upper few meters of the nucleus occurred.

For comet Bowell the observation that the grain temperature of 140 ± 10 K is consistent with the local blackbody temperature of 130 K suggests that $Q_a(a,\lambda,m) \equiv 1$ in the 1–20-μm wavelength region. If this is correct a total cross section of $(3 \pm 1) \times 10^8$ m^2 is found to lie within a 4.4-arcsec (1.16×10^7 m) diaphragm. The visual and near-infrared broadband data then lead to an estimated 1–2-μm geometric albedo of 0.14 ± 0.05, within the same diaphragm. That the absorption efficiencies are close to unity suggests that the mean grain size is even larger than that in comet Panther. By taking $a \gtrsim 10$ μm we find the total mass within the projected diaphragm to be $\gtrsim 4 \times 10^6$ kg. The estimated mass loss rate from the comet is then $\lesssim 70$ kg s^{-1}.

Broadband infrared observations of comet P/Stephan-Oterma have been reported by Veeder and Hanner (1981). They interpret their observations to rule out the presence of large numbers of submicron grains and grains of radius > 10 μm.

VII. INTERPRETATION OF THE INFRARED SPECTRA

In general the appearances of the near-infrared spectra of all three comets may result from the presence of both solid grains and/or free gaseous molecules and radicals in the cometary comae. We believe that solid grains are primarily responsible for the near-infrared spectral features in comets Panther and Bowell. First,

the two comets exhibit widely different degrees of gaseous emission in the visual, yet display identical near-infrared features; the infrared features are therefore not from gas. Second, the features are much broader than would be expected from a gaseous source (FWHM ~ 0.2 μm), suggesting that they originate in solid particles. This will be assumed through the remainder of the paper.

The near-infrared spectrum of the grains in the comae will depend upon the composition and crystallographic state of the grain material and on the grain size, temperature, and shape (Kieffer 1968). Effects due to multiple scattering between grains should be negligible since the comae are optically thin. In principle, grain-size-dependent scattering effects could produce substantial variations of reflectivity with wavelength, particularly if $x \sim 1$. However several arguments suggest that such scattering effects are small: (1) The broadband near-infrared and thermal infrared data suggest particle sizes in the range 2–4 μm for comet Panther and still larger sizes for comet Bowell. (2) Cometary grains seem to be highly irregular in shape (Brownlee 1978) and the irregularities would tend to smooth out reflectivity effects due to scattering. (3) The distribution of grain sizes would likewise degrade strong reflectivity effects due to scattering.

We therefore proceed on the basis that the shapes of the near-infrared spectra of the three comets result from the compositions of solid grains in the comae of these objects. Fine details of the spectra, in particular the depths of the absorption features, may reflect the influence of particle size and shape, however.

The near-infrared spectrum of P/Stephan-Oterma gives no evidence for the 2-μm absorption band of water ice (see Fig. 4). In order to place quantitative limits to the possible contribution of water ice to the P/Stephan-Oterma spectrum, elementary additive mixing calculations were performed. To simulate the reflective properties of refractory dust, a linear-reddened continuum was added to the water ice spectrum in various proportions. The slope of the continuum and the proportion of the dust relative to the water ice were varied until χ^2 was minimized between the model and the P/Stephan-Oterma spectra. It was found that not more than 20% of the near-infrared photons from the comet can have passed through large pure water ice grains. In view of the prevalence of water ice in all viable comet models, and especially in view of the suggestion from the visual data of a halo of subliming grains close to the nucleus of this comet, the absence of the strong water ice absorption seems initially surprising. The possibility that water ice is totally absent from the comet is consistent with the infrared data alone. However, the visual spectroscopic detection of H_2O^+ in this comet by Cochran *et al.* (1981) and the variation of the integrated brightness of the comet with heliocentric distance both suggest that water ice is present in the nucleus. The albedo of ice grains is mostly determined by refraction through their interiors, rather than by reflection from their surfaces. For this reason a small quantity of an absorbing contaminant in grains may suppress the overtones of fundamental vibration bands, especially those weaker features occurring at short wavelengths (Warren and Wiscombe 1981). The contamination of ice grains by small dust particles is a natural consequence of the standard comet nucleus models in which the two are taken to be closely mixed. Additionally, model calculations of the sublimation of *dirty* water ice grains of initial radius $a(0) \sim 100$ μm suggest an ice grain halo radius of $\lesssim 10^6$ m, consistent with the observed value 4×10^5 m. Pure ice grains would produce a much larger halo than is observed (Hanner 1980) as a result of the small absorptivity of ice in the visual region. Finally, the redness of the coma of comet P/Stephan-Oterma is contrary to the blueness of pure snows (O'Brien and Munis 1975), but is similar to the redness of many refractory materials where the color is often due to the Fe^{2+} ion. This again suggests contamination but it could also be a particle size effect.

In comets Bowell and Panther the absence of the water ice absorptions cannot be due to masking by a neutral absorbing contaminant since (other) discrete spectral features *are* present. It is implausible that a contaminant which is able to mask the strong water absorptions would simultaneously be unable to hide those of another molecule. Presumably the nonappearance of the water ice signature in the Bowell and Panther spectra shows that water ice is truly deficient in the coma grains of these comets. The results of additive mixing calculations indicate that not more than about 10% of the sunlight reflected from comets Bowell and Panther has passed through large pure water ice grains.

Attempts to identify the spectra with those of other solar system bodies have all failed. Some similarity to asteroid and meteorite reflectivities might be expected since in most comets an appreciable quantity of dust is present; typically half the cometary mass is in dust (Wyckoff 1982). The spectral features are not similar to any seen in the asteroids, the planets, planetary satellites, or in terrestrial or meteorite samples (Hunt and Salisbury 1970, 1971; Kieffer and Smythe 1974; Smythe 1975; Fink *et al.* 1976; Larson *et al.* 1979; Clark and McCord 1980; Lebofsky *et al.* 1981). A comparison with spectra of the interstellar medium and of objects in the cool interiors of molecular clouds has also proved fruitless. Similarity to interstellar dust spectra might be expected since, according to some workers (e.g., Greenberg 1980), comets may be aggregates of unaltered interstellar grains.

In Fig. 4 the comet spectra are compared with those of methane, ammonia, carbon dioxide, and water ices. Of these simple (and cosmically important) ices, the best match is with the wavelengths of overtones of vibration bands of ammonia. However, while there are general similarities with the ammonia ice spectrum, major differences exist in detail. Most importantly, the reflectivity minimum at 2.22 ± 0.02 μm in the comet spectra is significantly short of the ammonia minimum at 2.30 μm

(Slobodkin *et al.* 1978). Kieffer and Smythe (1974) place this band at 2.27 μm in 500-μm grains at a temperature of 77 K. Slobodkin *et al.* showed that the wavelengths of the above spectral features are not significantly altered by changing the temperature of the ammonia reflecting surface, neither do they depend appreciably on the crystallographic phase of the ammonia, though a fundamental absorption at ~ 3.1 μm does. In addition an absorption centered at 1.54 μm in the ammonia spectrum is completely absent from the comet spectra. The relative strengths of the ammonia absorption features do exhibit a dependence on the sample temperature and on the rate of crystal formation. At a sample temperature of 85 K, for instance, the 1.5-μm feature is all but absent, while the 2.04- and 2.30-μm features remain strong. Unfortunately the temperature of the grains in comet Panther (~ 250 K) is much higher than the 80 K at which the 1.54-μm absorption disappears. Hence based on the laboratory spectra it seems unlikely that temperature or other effects could be responsible for the differences between the ammonia and the comet spectra. The spectrum of ammonia hydrate ($NH_3 \cdot H_2O$) includes a strong contribution from H_2O and is therefore inconsistent with the comet spectra. Conceivably, if ammonia *is* present in the comets, blends with spectral bands of other materials might cause the band centers to shift to the observed positions. However, we cannot find any convincing candidate materials which reproduce the spectra of comets Panther or Bowell.

VIII. DISCUSSION

The existence and breakup of ammonia molecules in Panther would be consistent with the visual spectra of this object which show numerous lines due to NH_2. However, it is not clear that the solid grains in the comae of either of the comets can be composed only of ammonia ice since the lifetimes of such grains to sublimation would be very short. For instance at $R \sim 5$ AU, a distance similar to that of comet Bowell at the time of observation, the sublimation mass flux of NH_3 ice having a Bond albedo 0.5 would be $10^{-5.5}$ kg m^{-2} s^{-1}. With a density of 10^3 kg m^{-3}, even a 100-μm grain would have a lifetime to sublimation of only $10^{4.5}$ s. To travel $\sim 10^8$ m from the nucleus to the edge of the coma such a grain would have to be ejected from the nucleus at a speed $\sim 10^{3.5}$ m s^{-1}. Not only is this in excess of the speed suggested by the application of Eq. (3), it is ten times the sound speed in ammonia gas at the local blackbody temperature. In short, small ammonia grains would sublimate away too quickly to be detected and large grains would be propelled from the nucleus too slowly to reach far into the coma. These results become even more restrictive when more absorbing grains or smaller heliocentric distances are considered.

An alternative is that the observed absorptions do indeed result from overtones of vibrational transitions of the N–H bond but from within a different and less volatile molecule. Photodissociation of the molecule could still give rise to the NH_2 radical seen in the visual spectra. In addition to ammonia the interstellar medium is known to contain molecules of formamide and methylamine both of which include NH_2 and could be present in comets. Clearly the present data do not permit a unique identification of the material responsible for the near-infrared spectral features of comets Bowell and Panther. However, many materials are ruled out by the data, most importantly water and the simple ices.

According to some workers the initially simple chemistry of the comet nuclei (mostly H_2O, CO_2, and NH_3) is modified by interaction with the interstellar UV radiation and with the flux of galactic cosmic rays. Although the UV and cosmic-ray fluxes are very low, the 4.5×10^9-yr residence time of comets in the Oort cloud is sufficient to permit substantial concentrations of new molecules and radicals to build up. The mass of material involved in cosmic-ray reprocessing need not be large. Probably only the outermost few meters of the nucleus would undergo significant chemical transformation. Laboratory simulations of this chemical reprocessing have been performed by Moore (1981). Near-infrared spectra of the modified chemicals have been taken. Unfortunately, these spectra exist only for $\lambda > 3$ μm so that a comparison with our comet data is presently impossible (B. Donn 1981, private communication).

It may be that the near-infrared spectra of the comets Bowell and Panther record the presence of complex molecules on grains of a few μm radius in their comae. In fact, the hypothesis that "new" comets have unstable mantles of such molecules which are lost soon after the first perihelion is completely consistent with both the visual *and* the infrared observations of all three comets. Comets Bowell and Panther are both thought to be making their first approaches to the Sun as judged from their orbital characteristics. Both comets became active at large heliocentric distances. Comet Bowell possessed an extended dust coma at $R = 7$ AU and comet Panther has likewise been strongly active at large R. The similarities between these two comets in terms of their excess activity extend to their near-infrared reflection spectra. On the other hand, comet P/Stephan-Oterma was relatively inactive at *smaller* R, had a more simple photometric profile, and possibly a different near-infrared reflection spectrum. It is tempting to note that P/Stephan-Oterma is an older periodic comet which might easily have lost any supervolatile mantle it may once have possessed. It will be necessary to pursue the types of observation reported in the present work to encompass a larger sample of comets.

IX. SUMMARY

The observed properties of the comets P/Stephan-Oterma, Panther, and Bowell in the 0.5–3.0-μm region are all explainable by scattering of solar radiation from solid grains in their comae.

The visual surface brightness profile of comet P/Stephan-Oterma consists of two parts: a bright central re-

gion 4×10^5 m in radius is interpreted to be a halo of sublimating grains while an extended outer region is consistent with the presence of an isotropically expanding cloud of refractory grains. The near-infrared spectrum of the comet is featureless within the uncertainties of the measurements.

The visual surface brightness profile of comet Panther suggests the presence of sublimating grains in a halo having a radius 5×10^8 m centered on the nucleus. The grains in the central region of the coma have, depending on the actual value of the grain refractive index, a geometric albedo of 0.14 ± 0.05 and mean radii in the range 2–4 μm. At a heliocentric distance $R\sim1.9$ AU the grain mass loss rate from comet Panther was $\lesssim60$ kg s^{-1}. The 1.4–2.4-μm spectrum of comet Panther displays spectral features which are similar to features observed in laboratory spectra of solid NH_3, although there are significant differences. Micron-sized NH_3 grains would be unstable to sublimation in the coma of comet Panther and therefore the majority of the grains cannot consist of NH_3. The 2–4-μm grains most likely contain molecules which incorporate the N–H bond but which are more complex and less volatile than NH_3. Such molecules might be produced in the grains by cosmic-ray reprocessing.

The visual surface brightness profile of comet Bowell cannot be readily understood in terms of the simple models employed in the present study. The grains in comet Bowell have a similar albedo to those in comet Panther but have a larger mean radius (probably $\gtrsim10$ μm). At $R\sim4.5$ AU the grain mass loss rate was $\lesssim70$ kg s^{-1}. Near-infrared spectral features identical to those seen in comet Panther similarly suggest the presence of a molecule which incorporates the N–H bond.

We are grateful to J. Westphal and J. Gunn for permission to use the PFUEI and to J. Carrasco, S. Grollix, J. Hoessel, C. Porco, S. Staples, and G. Veeder for assistance with the observations. We thank J. Westphal and E. Ney for careful reading of the manuscript. D. Yeomans kindly provided ephemerides for the comets. This research was supported by NASA and NSF grants.

REFERENCES

A'Hearn, M. F., Dwek, E., and Tokunaga, A. T. (1981). Astrophys. J. **248**, L147–L151.
Arveson, J. C., Griffin, R. N., and Pearson, B. D. (1969). Appl. Opt. **8**, 2215–2232.
Becklin, E. E., and Westphal, J. A. (1966). Astrophys. J. **145**, 445–453.
Bobrovnikoff, N. (1954). Astron. J. **59**, 351–358.
Brownlee, D. E. (1978). In *Cosmic Dust*, edited by J. A. M. McDonnell (Wiley-Interscience, New York).
Burns, J. A. Lamy, P. L., and Soter, S. (1979). Icarus **40**, 1–48.
Clark, R. N., and McCord, T. B. (1980). Icarus **43**, 161–168.
Cochran, A. L., and Barker, E. S. (1981). In *Comets: Gases, Ices, Grains and Plasma*, IAU Colloquium No. 61, edited by L. L. Wilkening, Tucson, Arizona (University of Arizona Press, Tucson).
Cruikshank, D. P. (1980). Icarus **41**, 246–258.
Delsemme, A. H., and Miller, D. C. (1970). Planet. Space Sci. **18**, 717–730.
Delsemme, A. H., and Miller, D. C. (1971). Planet. Space Sci. **19**, 1229–1257.
Elias, J., Frogel, J., Matthews, K., and Neugebauer, G. (1982). Astron. J. **87**, 1029–1034.
Fink, U., Larson, H. P., Gautier, T. N., and Treffers, R. R. (1976). Astrophys. J. **207**, L63–L67.
Fink, U., and Sill, G. (1981). Abstract of a paper delivered at IAU Colloquium No. 61, *Comets: Gases, Ices, Grains and Plasma*, held in Tucson, Arizona, 1981.
Greenberg, J. M. (1976). Astrophys. Space Sci. **39**, 9–18.
Greenberg, J. M. (1980). In *Solid Particles in the Solar System*, IAU Symposium No. 90, edited by I. Halliday and B. A. McIntosh (Reidel, Dordrecht), pp. 343–350.
Gunn, J. E., and Westphal, J. A. (1981). Proc. Int. Soc. Opt. Eng. **290**, 16–23.
Hanner, M. S. (1980). In *Solid Particles in the Solar System*, IAU Symposium No. 90, edited by I. Halliday and B. A. McIntosh (Reidel, Dordrecht), pp. 223–236.
Hanner, M. S. (1981). Icarus **47**, 342–350.
Hasegawa, I., Nakano, S., and Yabushita, S. (1981). Mon. Not. R. Astron. Soc. **196**, 45P–46P.
Hunt, G. R., and Salisbury, J. W. (1970). Mod. Geol. **1**, 283–300.
Hunt, G. R., and Salisbury, J. W. (1971). Mod. Geol. **2**, 23–30.
Kieffer, H. H. (1968). Thesis, California Institute of Technology.
Kieffer, H. H., and Smythe, W. D. (1974). Icarus **20**, 506–512.
Larson, H. P., Feierberg, M. A., Fink, U., and Smith, H. A. (1979). Icarus **39**, 257–271.
Lebofsky, L. A., Rieke, G. H., and Lebofsky, M. J. (1981). Icarus **46**, 169–174.
Moore, M. H. (1981). Ph. D. thesis, submitted to University of Maryland.
Ney, E. P. (1975). In *The Study of Comets, Part* 1, NASA SP-393, edited by B. Donn (U.S. GPO, Washington, D.C.).
O'Brien, H. W., and Munis, R. H. (1975). Cold Regions Research and Engineering Laboratory, Research Report No. 332.
O'Dell, C. R. (1971). Astrophys. J. **166**, 675–681.
Oishi, M., Kawara, K., Kobayashi, Y., Maihara, T., Noguchi, K., Okuda, H., Sato, S., Iijima, T., and Ono, T. (1978). Publ. Astron. Soc. Jpn. **30**, 149.
Sekanina, Z. (1975). Icarus **25**, 218–238.
Sekanina, Z. (1982). Astrophys. J. **87**, 161–169.
Slobodkin, L. S., Buyakov, I. F., Cess, R. D., and Caldwell, J. (1978). J. Quant. Spectrosc. Radiat. Transfer **20**, 481–490.
Smythe, W. D. (1975). Icarus **24**, 421–427.
Thuan, T. X., and Gunn, J. E. (1976). Publ. Astron. Soc. Pac. **86**, 543–547.
Veeder, G. J., and Hanner, M. S. (1981). Icarus **47**, 381–387.
Warren, S. G., and Wiscombe, (1981). J. Atmos. Sci. **37**, 2712–2745.
Wehinger, P. A., Wyckoff, S., Herbig, G., Herzberg, G., and Lew, H. (1974). Astrophys. J. Lett. **190**, L43.
Whipple, F. L. (1950). Astrophys. J. **111**, 375.
Whipple, F. L. (1951). Astrophys. J. **113**, 464.
Wyckoff, S. (1982). In *Comets*, edited by L. L. Wilkening (University of Arizona Press, Tucson).